Nuclear Engineering and Technology 52 (2020) 337–343

Contents lists available at ScienceDirect

Nuclear Engineering and Technology

journal homepage: www.elsevier.com/locate/net

Original Article

Dislocation-oxide interaction in Y_2O_3 embedded Fe: A molecular dynamics simulation study

M. Mustafa Azeem [a], Qingyu Wang [a, *], Zhongyu Li [a], Yue Zhang [b]

[a] College of Nuclear Science and Technology, Fundamental Science on Nuclear Safety and Simulation Technology Laboratory, Harbin Engineering University, Harbin, 150001, China
[b] Nuclear and Radiation Safety Center, MEE, Beijing, 100082, China

ARTICLE INFO

Article history:
Received 21 January 2019
Received in revised form
1 July 2019
Accepted 9 July 2019
Available online 9 July 2019

Keywords:
Oxide dispersed strengthened (ODS) steel
Molecular dynamics (MD) simulation
Edge dislocation
Orowan loop
Dislocation dynamics

ABSTRACT

Oxide dispersed strengthened (ODS) steel is an important candidate for Gen-IV reactors. Oxide embedded in Fe can help to trap irradiation defects and enhances the strength of steel. It was observed in this study that the size of oxide has a profound impact on the depinning mechanism. For smaller sizes, the oxide acts as a void; thus, letting the dislocation bypass without any shear. On the other hand, oxides larger than 2 nm generate new dislocation segments around themselves. The depinning is similar to that of Orowan mechanism and the strengthening effect is likely to be greater for larger oxides. It was found that higher shear deformation rates produce more fine-tuned stress-strain curve. Both molecular dynamics (MD) simulations and BKS (Bacon-Knocks-Scattergood) model display similar characteristics whereby establishing an inverse relation between the depinning stress and the obstacle distance. It was found that $(110)_{oxide} \parallel (111)_{Fe}$ (oriented oxide) also had similar characteristics as that of $(100)_{oxide} \parallel (111)_{Fe}$ but resulted in an increased depinning stress thereby providing greater resistance to dislocation bypass. Our simulation results concluded that critical depinning stress depends significantly on the size and orientation of the oxide.

1. Introduction

The materials in advanced fission and fusion reactors entail higher-level strength in order to endure stringent irradiation criterion. Irradiation effects in structural materials are initiated by incident particles that result in production of point defects and dislocations. The atomic scale modeling provides a comprehensive mechanism to study properties of these materials and their defect interaction with obstacles. Therefore, a thorough understanding of defects' evolution can help in the selection of better radiation resistant materials, suitable for extended service conditions.

Fe-based ODS alloys are considered as one of the most promising candidate materials for advanced fission and fusion reactors due to their higher thermal stability, high temperature creep and corrosion resistance. It has been reported that radiation can affect the size of oxide along-with creation of amorphization [1–3]. Researchers concluded that oxide particles having ranges up to 3 nm act as coherent solute-enriched clusters while larger sizes act as near-stoichiometric complex particles [4]. As we know that dislocation obstacle interactions have profound effect on its mechanical properties. Therefore, mechanical properties and radiation resistance response of ODS steel significantly relies upon the size of oxide and achieving a higher understanding of dislocation nucleation in the radiation environment is crucial for determining the strength of any material [5,6]. The phenomenon of precipitate hardening enhance structural strengthening, but it increase embrittlement [7]. For the same reason, nature and mechanism of dislocation hindrance through presence of nano-oxides needs to be thoroughly explained [8,9].

Stress-driven dynamics of dislocation have been a topic of interest during the past decade [10,11]. Two kinds of interaction mechanisms have been reported in literature when investigating temperature effects [12]. One kind is that of the Orowan mechanism which is repulsive in nature while the second type exhibits attraction commonly at extreme temperatures in accordance with Srolovitz mechanism [12,13]. Climbing has also been observed when dislocation encounters a hard or non-shearable obstacle.

Terentyev et al. [14] mentioned that nature of the obstacle determines the interaction mechanism. They have found that the

* Corresponding author.
E-mail address: wangqingyu@hrbeu.edu.cn (Q. Wang).

https://doi.org/10.1016/j.net.2019.07.011

stress required to overcome any kind of obstacle present within a material depends upon size, orientation, temperature and composition of the oxide. Zhang et al. [15] pointed out that a material's yield strength is dependent on the size and number density of nano-sized precipitates as seen by APT and Cs-corrected TEM. Another critical factor effecting oxides' strengthening mechanism is intrinsic defects or defects produces during work hardening. During shear deformation, edge dislocations can emit or absorb Frenkel pairs which can make a dislocation climb. These F-pairs can be absorbed by dislocations which can later-on produce short segments of climbs around obstacles [16,17]. Lehtinen et al. [18] observed pinning and depinning mechanism during edge dislocation for different sizes and types of precipitates. They evaluated that the size transformation of oxides resulted in the advent of Orowan loop around it. It was observed that higher and consistent shear stress can multiply loops since the movement of dislocations is repelled by short-range stresses. For smaller oxides ($\leq$2 nm), the dislocations bypass without producing any loops around the oxides [10]. Dislocation dynamics results by Keyhani et al. [19] concluded that the motion of dislocation lines are similar to that of Orowan but it followed cutting mechanism as there was no observable loop when dislocation bypassed the precipitate.

Interaction of single/multiple edge/screw dislocations with Cu/Cr/C fine precipitates or voids in Fe and composite materials have been performed experimentally as well as through atomistic simulations [17,20–28]. MD simulations method is a significant tool in comprehending the mechanism caused by dislocation interactions and nucleation in composite materials as it is a challenging task to analyze it experimentally [29–31]. During atomistic simulations by Osetsky et al. [27], size variations of oxides were found to have a profound effect on dislocation-precipitates/void interaction mechanism. Dérès et al. [32] discovered that dislocation interactions with nano-voids could be a probable cause of radiation hardening in alpha Fe. Additionally, it was demonstrated that critical shear resolved stress (CRSS) is inversely proportional to the inter obstacle distance whilst establishing obstacle size dependence on depinning mechanism. Meanwhile, Proville et al. [33] investigated size effects on dislocation depinning mechanism in FCC metals and compared their atomistic simulation results with BKS theoretical model. Xiang et al. [34] reported that dislocation-obstacle interaction is also dependent on their relative location and distance. Singh et al. [35] performed atomistic simulation of edge dislocation interaction and found out that critical shear stress and strengthening mechanism predominantly depends upon size as well as orientation of the oxide/Fe.

Although numerous MD simulations and relative studies have been performed on the strengthening effects of Fe with different nano-sized obstacles [10,14,18,36–53]. To the best of authors' knowledge, Fe embedded Y_2O_3 oxides have been not reported hitherto.

In the present study, we have performed MD simulations to study the interaction between a single edge dislocation and Y_2O_3 in Fe-based ODS composite model. The study specifically considered the effect of oxides' sizes, deformation speed and orientation of oxide-Fe interface. Furthermore, interaction mechanism for each size was also analyzed. Critical depinning stress for $(100)_{oxide}$ || $(111)_{Fe}$ model was calculated by BKS model. Subsequently, critical depinning stress for $(110)_{oxide}$ || $(111)_{Fe}$ model was also calculated to form a comprehensive relative analysis of the two models. Our results are in accordance with the simulation studies reported by the relevant literatures. The computational details have been described in the next section, followed by results and discussion part.

2. Computational details

All MD simulations are performed with LAMMPS code [54]. The crystal structure of Y_2O_3 is cubic with space group Ia-3, having body-centered symmetry of 80 atoms in each unit cell. The 32 Y atoms in the structure occupy 8(b) & 24(d) sites while 48 O atoms are positioned on 48(e) general sites respectively [55]. Y_2O_3 has a lattice constant of 1.06 nm as reported by Hanic et al. [56]. In our simulation the most stable structure of Y_2O_3 lattice parameter was achieved at 1 nm. Fe has a BCC structure with lattice parameter of 0.2886 nm. Initially, Y_2O_3 is relaxed for 30 ps at 300 K by NPT ensemble. Y_2O_3 is a type of ionic crystal. Various properties of Y_2O_3 have been elaborated in detail by the original charge model potential and further substantiated by various researchers [5,57–60]. While conducting thermal relaxation, the model's structural stability is enhanced by setting valence charges as electronic charge i.e. Y (+3) and O (−2).

By following the method of Bacon and co-authors [61], initial coordinate axes of the Fe box are oriented along [111], [−1-12] and [1–10] directions. Queyreau [62] discussed that in BCC Fe, favorable dislocations exist in {110} and {112} planes. An edge dislocation with Burgers vector $\mathbf{b} = a/2[111]$ in (110) slip plane has been created by deleting a layer of Fe atoms. Thermal relaxation procedure is performed through NPT ensemble at 300 K for 50 ps

Initially, distance between dislocation core in Fe and the center of oxide is equal to 7.25 nm which is nearly one quarter of Lx. Before further relaxation, a few Fe atoms within the range of 0.2 nm at oxide - Fe interface have been deleted to avoid overlapping. The composite model is relaxed again for another 50 ps at same temperature with periodic boundary conditions (PBC) applied in all directions. However, we introduced some free space at x and z boundaries since PPPM summation method requires periodic boundaries for electrostatic interactions. In LAMMPS, the pair style for long-range coulombic interaction is solved by performing computation in K-space which uses particle-particle particle-mesh (PPPM) solver method for optimization of charged model.

The shear deformation simulations are performed on an edge dislocation model having different oxide sizes embedded at center of the simulation box. The shear deformation of the simulation box is calculated by using $\tau = F_x/A_{xy}$ where F_x is shear deformation applied along x-axis and A_{xy} is area in xy plane. The simulation box is divided into three portions i.e. upper, lower, and middle. The upper and lower parts are kept rigidly fixed while the middle part is mobile during simulation. The shear deformation is applied on upper part of the box by moving it with different speeds along the x-direction. The edge dislocation is set in motion due to relative displacement between upper side and the rest of simulation box.

In the second part of our study, simulation for the orientation effect of oxide (4 nm) was investigated in the same manner. In composite model, the orientation of Y_2O_3 is either [100]-[010]-[001], (denoted as $(100)_{oxide}$ || $(111)_{Fe}$) or [101]-[010]-[-101] (denoted as $(110)_{oxide}$ || $(111)_{Fe}$). The latter one is dominant interface orientation correlation in ODS steel as reported by Klimiankou et al. [63].

The schematic diagram prior to applied deformation is illustrated in Fig. 1. Table 1 shows the detail of each model under our study. The evolution of atomic structure was analyzed by Visualization tool OVITO and DXA module (Dislocation Extraction Algorithm) was used to analyze the dislocation core, its movement and Burgers vector calculation [64].

The choice of interatomic potential is the most crucial parameter for modeling in MD simulations. For an effective MD simulation, it is necessary that interatomic potential should be computationally effective and should reproduce the physical properties of a material. But only a limited number of interatomic

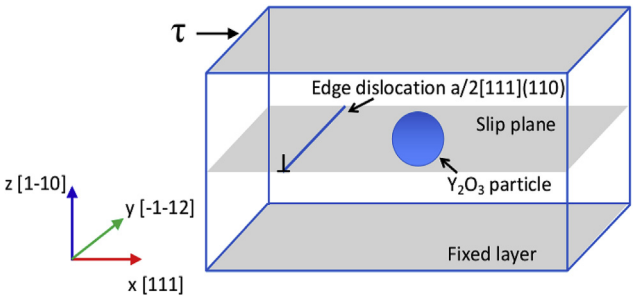

Fig. 1. Schematic representation of the simulation setup containing an edge dislocation, a slip plane and a Y_2O_3 oxide at center.

potentials are being reported for Fe–Y–O composite materials [58,59,65–67]. Out of these limited choices, interatomic potentials formulated by Hammond et al. [67] was found to be the most appropriate. This empirical pairwise potential was originally designed to offer a tractable method Fe–Y–Ti–O system with economical computational cost and its cohesive energy and energy per atoms are consistent with DFT calculations. In order to ensure reliable performance of our model with aforementioned potential, we performed multiple simulations to test structural stability of Fe, Y_2O_3 and their composites. We also found this potential to be the most suitable one for our case.

3. Results and discussion

3.1. Effect of size and mechanism

The effects of oxide sizes on depinning mechanism is clearly represented in Fig. 2(a–d) in which oxides of different sizes and their interaction mechanism are shown. DXA analysis of different time steps for size 2 nm shows that dislocation line bows around the oxide without entering it. In this case, the oxide acts as a void due to partial absorption of dislocation and no shearing within the oxide is seen post bypass (Fig. 2 (a)). For oxide sizes greater than 2 nm, new dislocation segments are generated during shearing as indicated in Fig. 2(b–d) which would apparently act as further obstacle for subsequent dislocation motions. It is evident that a part of the dislocation line facing oxide has been bowing-out while the other part keeps on moving due to applied deformation. Before detaching from the oxide, a dipole is formed around it and after depinning dislocation line moves freely. We have observed that the dislocation is trapped around the oxide and generates dislocation loops similar to Orowan mechanism. It should be mentioned that the presence of perfect spherical Orowan loops around the obstacle has been rarely reported in experimental studies because they have a higher strain energy than normal straight dislocations [68,69].

Table 1
Distribution details of each model under study with their composition.

Y_2O_3 diameter (nm)	Atoms in oxide	Dimension (in lattice spacing)	Total number of atoms for $(100)_{oxide}$ || $(111)_{Fe}$	Total number of atoms for $(110)_{oxide}$ || $(111)_{Fe}$
2	43	60 × 40 × 40	766915	-
3	180	60 × 40 × 40	766866	-
4	391 (384 for $(110)_{oxide}$ || $(111)_{Fe}$)	60 × 40 × 40	766826	766821
		60 × 50 × 40	958558	988549
		60 × 60 × 40	1150296	1150274
		60 × 70 × 40	1342046	1342034
		60 × 80 × 40	1533735	1533747
6	1311	60 × 40 × 40	766716	-

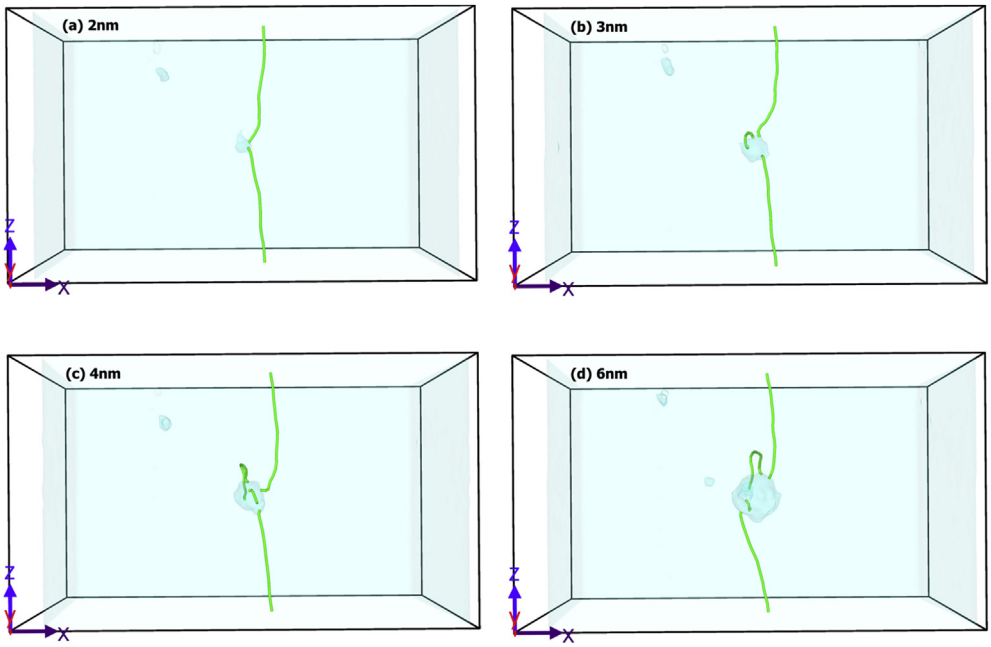

Fig. 2. MD snapshots for edge dislocation depinning separated by L=(Ly-d) nm where Ly is the length of Y axis and d the diameter of the oxide.

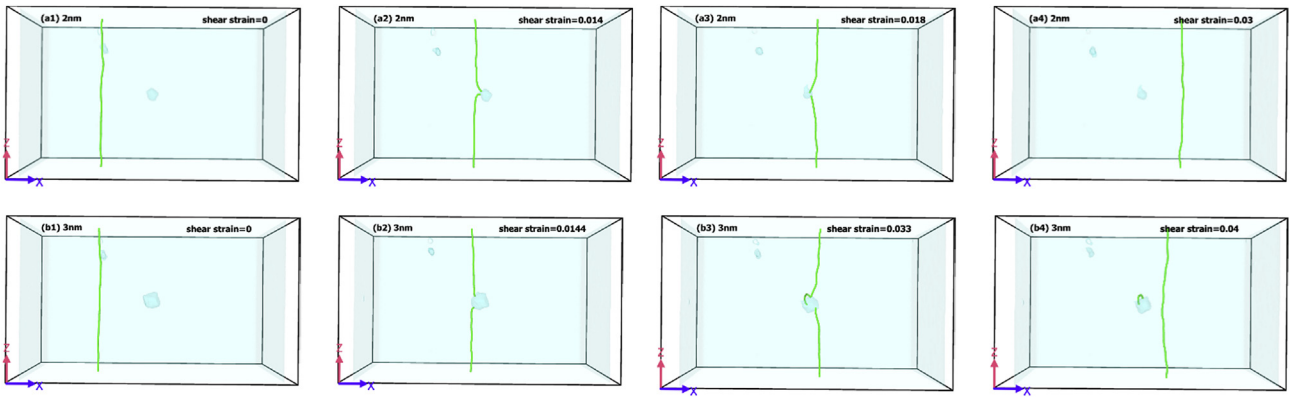

Fig. 3. Atomic reaction mechanism between dislocation and oxides' initial position, pinning, depinning and after bypass for 2 nm, 3 nm composite model.

Fig. 2 displays dislocation depinning interaction mechanism of different oxides with 0.01 nm/ps deformation speed at 300 K, where (a), (b), (c), (d) represent 2, 3, 4, 6 nm diameter oxides with different strains i.e. 0.018, 0.033, 0.045, 0.055, respectively. The defects at the top of MD snapshots are point defects formed during creation of dislocation. Granberg et al. [36] investigated the interaction of an edge dislocation with carbide precipitates in Fe matrix of different shapes and detected the formation of Orowan loops around spherical precipitates of sizes greater than 2 nm. They also pointed out that larger precipitate sizes follow Orowan depinning mechanism [6,36] which is in agreement with our results.

Lehtinen et al. [18] mentioned that any precipitate size less than 2 nm should be considered as a weak obstacle. While for sizes more than 2 nm, Orowan loop was not absorbed after dislocation bypass. The compression induced by strain energy of larger precipitate may cause a rising curvature of dislocation line during bow-out. Our simulation results clearly demonstrate that the interaction mechanism is size dependent as depicted in Fig. 2. It can be seen that larger oxide particles result in higher depinning stress which could be a reason for enhanced strengthening effects as reported by Li et al. [31]. During initial stage of larger oxides dislocation interaction, local stress fields are produced as a result of lattice mismatch and dislocation exits. Therefore, during shear deformation of Fe matrix, higher compressive stresses are created which produce dislocation loops around the oxide and results in enhanced strengthening effect.

Fig. 3 demonstrates oxide-dislocation atomic reaction mechanism at 0.01 nm/ps deformation speed along its shear strains. In Fig. 3 (a1-a4), atomic reaction mechanism is shown for 2 nm oxide during its interaction at 0, 0.014, 0.018 and 0.03 shear strains respectively. Similarly, Fig. 3(b1-b4) represents atomic reaction mechanism for 3 nm at 0, 0.0144, 0.033, and 0.04 shear strain respectively. For sizes more than 2 nm, depinning dislocation follow an Orowan loop. Furthermore, higher strain rate is experienced for larger oxides and vice versa.

3.2. Effect of deformation speed

When deformation is applied, dislocation starts to move along the slip plane and this movement is affected by loading speed. If applied deformation is increased, oxide-dislocation interaction reaches a transitional phase during which we can easily observe its interaction mechanism. Fig. 4 illustrate stress-strain plots for model having 4 nm embedded oxide particle sheared with different deformation speeds. The stress-strain curves in Fig. 4 do not show any obvious elastic-plastic transition other than a higher strain hardening. Lehtinen et al. [18] used first stress drop as the critical depinning stress. However, MD snapshots for our case reveals that the second stress drop corresponds to critical depinning stress. For red & blue curves shown in Fig. 4(a), A_r, B_r and C_r correspond to 0.01 nm/ps deformation speed while A_b, B_b and C_b correspond to 0.05 nm/ps deformation speed with each A, B and C denotes touching, depinning and bypass respectively. In Fig. 4(a), lower deformation speed of 0.001 nm/ps is shown by black curve which has a considerably lower strain rate. Critical depinning stress for 0.01 nm/ps, 0.05 nm/ps and 0.001 nm/ps deformation speeds are 1.8 GPa, 3.4 GPa and 0.5 GPa respectively. This reveals that critical depinning stress is also directly proportional to the deformation speed.

Our simulation results show that depinning stress is different for different deformation speeds. Obviously, higher deformation speed results in a higher level of depinning stress. This is because the oxide surrounded by Orowan loop creates greater hindrance for dislocation movement. Simultaneously, multiple dislocation loops increase the effective size of the oxide which will improve strain hardening. Curve deviations found in Fig. 4(a) are due to bonding

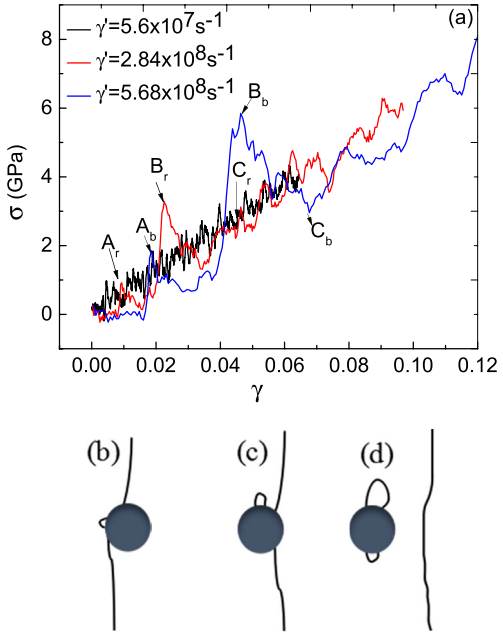

Fig. 4. (a) Stress-strain for [111] direction curves for an edge dislocation with varying strain rates $\dot{\gamma}$ for 4 nm oxide models. (b)–(d) represent the interaction phases for A_r, B_r and C_r in (a).

and debonding of atoms near the interface of oxide and dislocation. With the passage of time, multiple bonding and debonding of dislocations with oxides, Fe and their interfaces will eventually lead to higher critical depinning stress. OVITO visualizations show that when the dislocation moves closer to the oxide along (110) slip plane, the attraction between them become stronger. Therefore, dislocation gliding encounters greater resistance and this in turn increases the amount of stress required for plastic deformation. Moreover, our strain rates are comparable to that reported by authors [10,18,37]. Queyreau et al. [68] observed that higher deformation speeds cause multiple Orowan loops which invariably leads to higher loop size. A similar kind of mechanism is seen during the interaction of Cu precipitates in bcc Fe [70].

3.3. Critical depinning stress

The critical shear stress is usually measured as a function of critical angle between dislocation depinning arms called critical resolved shear stress (CRSS) and is dependent on Peierls stress [71]. Russell et al. [72] has mentioned that angle for depinning arms could have a relation with dislocation's energy on either side of the matrix-precipitate interface if the precipitate is softer than the matrix. In our case, dislocation segments after depinning are almost parallel while assuming that oxides are hard spheres. Therefore, we have used Bacon-Knocks-Scattergood (BKS) model [73] to calculate the critical depinning stress where periodic array of obstacles are considered. BKS model takes the form of:

$$\sigma_c = C\frac{Gb}{L-D}[ln(\frac{\overline{D}}{b}) + 0.7] \quad (1)$$

where C = 1/2π, L is the distance between two obstacles, D is diameter of the obstacle, $\overline{D}$ is harmonic average of L and D given by $\overline{D} = \frac{DL}{D+L}$,G is shear modulus, b is magnitude of Burgers vector. The value of impenetrable obstacle like oxide is taken as 0.7. Here, b = 0.2499 nm and D = 4 nm because (1) is practicable for sizes greater than 2 nm [6].

In order to obtain elastic parameter for Fe, we have simulated a smaller box containing ~10000 atoms at very low deformation speed (0.001 nm/ps). Furthermore, it has been linearly fitted to obtain anisotropic shear modulus ($G_{\langle 111\rangle}$) which was found to be 59.89 GPa, comparable with other studies [18,74,75].

The distance L between two oxide obstacles is calculated by measuring the distance between oxide and its mirror counterpart along Y-axis of the simulation box. Therefore, L = Ly - d, where Ly is the length of Y axis and d is diameter of oxide. To draw a comparison between MD simulation results and BKS model, spherical oxide diameters in range of 2–6 nm was used while L was varied between 14.4 and 38 nm. To determine the effect of L, we followed the procedure mentioned earlier except now we varied the atomic planes having infinite periodic obstacles. Oxide size of 4 nm with 0.05 nm/ps deformation speed was selected for this analysis as depicted in Fig. 5.

Fig. 5 shows the critical depinning stress (σ_c) obtained from MD simulation of $(100)_{oxide}$ || $(111)_{Fe}$ and $(110)_{oxide}$ || $(111)_{Fe}$ along with values of BKS model. Although MD simulation results have higher values (≈5 times) than BKS model but the trend of critical stress is similar in both models *i.e.* σ_c has an inverse dependence on L and same is consistent with results reported in literature [18,26]. It is worth mentioning that higher values of σ_c obtained by MD simulations are in contrast to the results calculated by Lehtinen et al. [18]. The main reason for contradiction between the two studies is due to different nature of obstacles and interatomic potentials. We considered oxide as hard impenetrable obstacle. Therefore, higher stress is required for the dislocation to bypass which is the primary

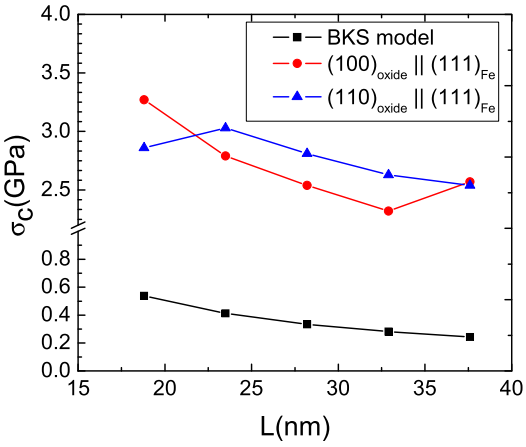

Fig. 5. Plots of MD simulations and BKS equation for critical depinning stress σ_c as a function of distance between two oxides.

reason for strengthening effect in ODS steel. It can be further noted that $(110)_{oxide}$ || $(111)_{Fe}$ model require comparatively higher stress for depinning than $(100)_{oxide}$ || $(111)_{Fe}$. Therefore, it is proposed that by optimizing oxide size and orientation, strengthening effect of ODS steel can be enhanced.

Dislocation Dynamics (DD) simulation can help to fully understand the underlying mechanism of dislocation interaction by considering the mobility law at extended scales. We have also presumed that MD simulation when coupled with large-scale dislocation dynamics simulation can be beneficial in studying the fundamental mechanisms between elastic-plastic phases in ODS steel. The driving force of dislocation line can be obtained through Peach–Koehler expression by considering the individual dislocations by the stress field of inter dislocations [44],76]. MD simulations are also capable of providing mobility of dislocations [38,45],77] if a linear relation is considered between applied deformation and dislocation velocity as implemented in Paradis [46]. Consequently, multiple dislocations and their interactions can be simulated on larger scales in DD by taking the data from MD simulation.

4. Conclusion

In this study, we carried out molecular dynamics simulations to investigate oxide-dislocation interaction mechanisms based on sizes, deformation speeds and orientation in ODS steel models. We have concluded that these factors play a major role in depinning mechanism. In case of oxide sizes <2 nm, our simulation results demonstrate that dislocation follows Orowan depinning mechanism without leaving any dislocation loop. On the other hand, any size ≥2 nm produces new dislocations segments which increase obstacle as well as material strength. Likewise, high deformation speed results in more dislocation loops and invariably enhance strengthening. Moreover, $(110)_{oxide}$ || $(111)_{Fe}$ interface requires a higher depinning stress for the obstacles to bypass. Our results exhibit a good correlation with simulations performed by different researchers on precipitate hardening and dislocation interactions of their respective models. Since Fe in the present model is dominant, so exchanging Fe–Fe potential by using many body style like EAM or MEAM can have new and interesting results. Therefore, further research on potentials for Fe–Y_2O_3 systems is required.

Conflicts of interest

The authors declare that they have no conflicts of interest.

Acknowledgments

The authors thank Dr. Lin. Shao from Texas A & M University for discussions and suggestions. M.Mustafa Azeem would like to thank Chinese Scholarship Council (CSC) and Harbin Engineering University for their International Scholarship program. Qingyu Wang acknowledges High Performance Center of Harbin Engineering University. This work is partially supported by National Science Foundation of China (Grant No. 11505037) and Fundamental Research Funds for the Central Universities (HEUCFJ171502 and 3072019CF1502).

Appendix A. Supplementary data

Supplementary data related to this article can be found at https://doi.org/10.1016/j.net.2019.07.011.

References

[1] J.P. Wharry, M.J. Swenson, K.H. Yano, A review of the irradiation evolution of dispersed oxide nanoparticles in the b.c.c. Fe-Cr system: current understanding and future directions, J. Nucl. Mater. 486 (2017) 11–20, https://doi.org/10.1016/j.jnucmat.2017.01.009.
[2] S. Ukai, M. Fujiwara, Perspective of ODS alloys application in nuclear environments, J. Nucl. Mater. 307–311 (2002) 749–757, https://doi.org/10.1016/S0022-3115(02)01043-7.
[3] S.J. Zinkle, G.S. Was, Materials challenges in nuclear energy, Acta Mater. 61 (2013) 735–758, https://doi.org/10.1016/j.actamat.2012.11.004.
[4] L. Yang, Y. Jiang, G.R. Odette, W. Zhou, Z. Liu, Y. Liu, Nonstoichiometry and relative stabilities of Y2Ti2O7polar surfaces: a density functional theory prediction, Acta Mater. 61 (2013) 7260–7270, https://doi.org/10.1016/j.actamat.2013.08.031.
[5] M. Dholakia, S. Chandra, S.M. Jaya, A comparative study of topology and local disorder in Y2O3, Y2TiO5, and Y2Ti2O7 crystals Manan, J. Alloy. Comp. 739 (2018) 1037–1047, https://doi.org/10.1016/j.jallcom.2017.12.244.
[6] Y.N. Osetsky, D.J. Bacon, An atomic-level model for studying the dynamics of edge dislocations in metals, Model. Simul. Mater. Sci. Eng. 11 (2003) 427–446, https://doi.org/10.1088/0965-0393/11/4/302.
[7] D.A. Terentyev, G. Bonny, L. Malerba, Strengthening due to coherent Cr precipitates in Fe-Cr alloys: atomistic simulations and theoretical models, Acta Mater. 56 (2008) 3229–3235, https://doi.org/10.1016/j.actamat.2008.03.004.
[8] L.K. Mansur, A.F. Rowcliffe, R.K. Nanstad, S.J. Zinkle, W.R. Corwin, R.E. Stoller, Materials needs for fusion, Generation IV fission reactors and spallation neutron sources - similarities and differences, J. Nucl. Mater. (2004) 329–333, https://doi.org/10.1016/j.jnucmat.2004.04.016, 166–172.
[9] K.L. Murty, I. Charit, Structural materials for Gen-IV nuclear reactors: challenges and opportunities, J. Nucl. Mater. 383 (2008) 189–195, https://doi.org/10.1016/j.jnucmat.2008.08.044.
[10] A. Lehtinen, L. Laurson, F. Granberg, K. Nordlund, M.J. Alava, Effects of precipitates and dislocation loops on the yield stress of irradiated iron, Sci. Rep. 8 (2018) 1–12, https://doi.org/10.1038/s41598-018-25285-z.
[11] S. Kodambaka, S.V. Khare, W. Święch, K. Ohmori, I. Petrov, J.E. Greene, Dislocation-driven surface dynamics on solids, Nature 429 (2004) 49–52, https://doi.org/10.1038/nature02495.
[12] Y. Ijiri, N. Oono, S. Ukai, H. Yu, S. Ohtsuka, Y. Abe, Y. Matsukawa, Consideration of the oxide particle–dislocation interaction in 9Cr-ODS steel, Philos. Mag. A 97 (2017), https://doi.org/10.1080/14786435.2017.1288942.
[13] D.J. Srolovitz, R.A. Petkovic-luton, M.J. Litton, Diffusional relaxation of the dislocation-inclusion repulsion, Philos. Mag. A Phys. Condens. Matter, Struct. Defects Mech. Prop. 48 (1983) 795–809, https://doi.org/10.1080/01418618308236545.
[14] D. Terentyev, G. Bonny, C. Domain, G. Monnet, L. Malerba, Mechanisms of radiation strengthening in Fe-Cr alloys as revealed by atomistic studies, J. Nucl. Mater. 442 (2013) 470–485, https://doi.org/10.1016/j.jnucmat.2013.03.054.
[15] Z. Zhang, C.T. Liu, M.K. Miller, X.L. Wang, Y. Wen, T. Fujita, A. Hirata, M. Chen, G. Chen, B.A. Chin, A nanoscale co-precipitation approach for property enhancement of Fe-base alloys, Sci. Rep. 3 (2013) 1–6, https://doi.org/10.1038/srep01327.
[16] D. Hull, D.J. Bacon, Indroduction to Dislocations, fifth ed., Butterworth-Heinemann, 2011.
[17] D. Terentyev, P. Grammatikopoulos, D.J. Bacon, Y.N. Osetsky, Simulation of the interaction between an edge dislocation and a < 1 0 0> interstitial dislocation loop in Alpha-iron, Acta Mater. 56 (2008) 5034–5046, https://doi.org/10.1016/j.actamat.2008.06.032.
[18] A. Lehtinen, F. Granberg, L. Laurson, K. Nordlund, M.J. Alava, Multiscale modeling of dislocation-precipitate interactions in Fe: from molecular dynamics to discrete dislocations, Phys. Rev. E. 93 (2016) 1–9, https://doi.org/10.1103/PhysRevE.93.013309.
[19] A. Keyhani, R. Roumina, Dislocation-precipitate interaction map, Comput. Mater. Sci. 141 (2018) 153–161, https://doi.org/10.1016/j.commatsci.2017.09.036.
[20] A. Takahashi, N.M. Ghoniem, A computational method for dislocation-precipitate interaction, J. Mech. Phys. Solids 56 (2008) 1534–1553, https://doi.org/10.1016/j.jmps.2007.08.002.
[21] S. Kondo, T. Mitsuma, N. Shibata, Y. Ikuhara, Direct observation of individual dislocation interaction processes with grain boundaries, Sci. Adv. 2 (2016) 1–8, https://doi.org/10.1126/sciadv.1501926.
[22] I. Ringdalen, S. Materials, N. Trondheim, Dislocation dynamics study of precipitate hardening in Al – Mg – Si alloys with input from experimental characterization, MRS Commun. (2017) 1–8, https://doi.org/10.1557/mrc.2017.78.
[23] A.V. Bakaev, D.A. Terentyev, P.Y. Grigorev, E.E. Zhurkin, Atomistic simulation of the interaction between mobile edge dislocations and radiation-induced defects in Fe-Ni-Cr austenitic alloys, J. Surf. Investig. X-Ray, Synchrotron Neutron Tech. 8 (2014), https://doi.org/10.1134/S1027451014020062.
[24] Y. Long, N.X. Chen, Atomistic Simulation of Misfit Dislocation in Metal/Oxide Interfaces 42, 2008, pp. 426–433, https://doi.org/10.1016/j.commatsci.2007.08.007.
[25] F. Granberg, Interaction Mechanisms of Edge Dislocations with Obstacles in Fe and Metal Alloys, 2016.
[26] D. Terentyev, G. Bonny, C. Domain, G. Monnet, L. Malerba, Mechanisms of radiation strengthening in Fe – Cr alloys as revealed by atomistic studies, J. Nucl. Mater. 442 (2013) 470–485, https://doi.org/10.1016/j.jnucmat.2013.03.054.
[27] Y.N. Osetsky, D.J. Bacon, V. Mohles, Atomic modelling of strengthening mechanisms due to voids and copper precipitates in α-iron, Philos. Mag. A 83 (2003) 3623–3641, https://doi.org/10.1080/14786430310001603364.
[28] Y.N. Osetsky, A.G. Mikhin, A. Serra, Computer simulation study of copper precipitates in α-iron, J. Nucl. Mater. 212–215 (1994) 236–240, https://doi.org/10.1016/0022-3115(94)90063-9.
[29] C.S. Becquart, C. Domain, Modeling microstructure and irradiation effects, Metall. Mater. Trans. A 42 (2011) 852–870, https://doi.org/10.1007/s11661-010-0460-7.
[30] A. Simar, H.J.L. Voigt, B.D. Wirth, Molecular dynamics simulations of dislocation interaction with voids in nickel, Comput. Mater. Sci. 50 (2011) 1811–1817, https://doi.org/10.1016/j.commatsci.2011.01.020.
[31] J. Li, B. Liu, Q.H. Fang, Z.W. Huang, Y.W. Liu, Atomic-scale strengthening mechanism of dislocation-obstacle interaction in silicon carbide particle-reinforced copper matrix nanocomposites, Ceram. Int. 43 (2017) 3839–3846, https://doi.org/10.1016/j.ceramint.2016.12.040.
[32] J. Dérès, L. Proville, M.C. Marinica, Dislocation depinning from nano-sized irradiation defects in a bcc iron model, Acta Mater. 99 (2015) 99–105, https://doi.org/10.1016/j.actamat.2015.07.067.
[33] L. Proville, B. Bakó, Dislocation depinning from ordered nanophases in a model fcc crystal: from cutting mechanism to Orowan looping, Acta Mater. 58 (2010) 5565–5571, https://doi.org/10.1016/j.actamat.2010.06.018.
[34] Y. Xiang, D.J. Srolovitz, L.-T. Cheng, E. Weinan, Level set simulations of dislocation-particle bypass mechanisms, Acta Mater. 52 (2004) 1745–1760. https://doi.org/10.1016/j.actamat.2003.12.016.
[35] C.V. Singh, D.H. Warner, Mechanisms of Guinier-Preston zone hardening in the athermal limit, Acta Mater. (2010), https://doi.org/10.1016/j.actamat.2010.06.055.
[36] F. Granberg, D. Terentyev, K. Nordlund, Interaction of dislocations with carbides in BCC Fe studied by molecular dynamics, J. Nucl. Mater. 460 (2015) 23–29, https://doi.org/10.1016/j.jnucmat.2015.01.064.
[37] F. Granberg, D. Terentyev, K. Nordlund, Interaction of dislocations with carbides in BCC Fe studied by molecular dynamics, Fusion Sci. Technol. 66 (2014) 23–29, https://doi.org/10.1016/j.jnucmat.2015.01.064.
[38] X.H. Long, D. Wang, W. Setyawan, P. Liu, N. Gao, R.J. Kurtz, Z.G. Wang, X.L. Wang, Atomistic simulation of interstitial dislocation loop evolution under applied stresses in BCC iron, Phys. Status Solidi Appl. Mater. Sci. 215 (2018) 1–5, https://doi.org/10.1002/pssa.201700494.
[39] X. Zhang, H. Deng, S. Xiao, X. Li, W. Hu, Atomistic simulations of solid solution strengthening in Ni-based superalloy, Comput. Mater. Sci. 68 (2013) 132–137, https://doi.org/10.1016/j.commatsci.2012.10.002.
[40] X. Zhang, G. Lu, How Cr changes the dislocation core structure of α-Fe: the role of magnetism, J. Phys. Condens. Matter 25 (2013), https://doi.org/10.1088/0953-8984/25/8/085403.
[41] K. Yasunaga, M. Iseki, M. Kiritani, Dislocation structures introduced by high-speed deformation in bcc metals, Mater. Sci. Eng. A 350 (2003) 76–80, https://doi.org/10.1016/S0921-5093(02)00697-4.
[42] Z. Huang, J.E. Allison, A. Misra, Interaction of glide dislocations with extended precipitates in Mg-Nd alloys, Sci. Rep. 8 (2018) 1–12, https://doi.org/10.1038/s41598-018-20629-1.
[43] D. Terentyev, D.J. Bacon, Y.N. Osetsky, Interaction of an edge dislocation with voids in α-iron modelled with different interatomic potentials, J. Phys. Condens. Matter 20 (2008), https://doi.org/10.1088/0953-8984/20/44/445007.
[44] D. Terentyev, P. Grammatikopoulos, D.J. Bacon, Y.N. Osetsky, Simulation of the interaction between an edge dislocation and a ⟨1 0 0⟩ interstitial dislocation loop in α-iron, Acta Mater. 56 (2008) 5034–5046, https://doi.org/10.1016/j.actamat.2008.06.032.
[45] C.S. Shin, M.C. Fivel, M. Verdier, K.H. Oh, Dislocation-impenetrable precipitate interaction: a three-dimensional discrete dislocation dynamics analysis,

Philos. Mag. A 83 (2003) 3691–3704, https://doi.org/10.1080/14786430310001599379.
[46] M.V. Rodriguez, P.J. Ficalora, The Mechanism of a Hydrogen - Dislocation Interaction in B. C.C. Metals : embrittlement and Dislocation Motion 85, 1987, pp. 43–52.
[47] F. Granberg, Interaction Mechanisms of Edge Dislocations with Obstacles in Fe and Metal Alloys, 2016.
[48] M. Popova, Y.L. Shen, T.A. Khraishi, Atomistic simulation of dislocation interactions in a model crystal subjected to shear, Mol. Simul. 31 (2005) 1043–1049, https://doi.org/10.1080/08927020500349999.
[49] G. Bonny, A. Bakaev, D. Terentyev, E. Zhurkin, M. Posselt, Atomistic study of the hardening of ferritic iron by Ni-Cr decorated dislocation loops, J. Nucl. Mater. 498 (2018) 430–437, https://doi.org/10.1016/j.jnucmat.2017.11.016.
[50] T. Hatano, H. Matsui, Molecular dynamics investigation of dislocation pinning by a nanovoid in copper, Phys. Rev. B Condens. Matter 72 (2005) 1–8, https://doi.org/10.1103/PhysRevB.72.094105.
[51] G. Monnet, Multiscale modeling of precipitation hardening: application to the Fe-Cr alloys, Acta Mater. 95 (2015) 302–311, https://doi.org/10.1016/j.actamat.2015.05.043.
[52] J. Xu, C. Wang, W. Zhang, C. Ren, H. Gong, P. Huai, Atomistic simulations of the interactions of helium with dislocations in nickel, Nucl. Mater. Energy 7 (2016) 12–19, https://doi.org/10.1016/j.nme.2016.02.007.
[53] E. Martínez, D. Schwen, A. Caro, Helium segregation to screw and edge dislocations in α-iron and their yield strength, Acta Mater. 84 (2015) 208–214, https://doi.org/10.1016/j.actamat.2014.10.066.
[54] S. Plimpton, Fast parallel algorithms for short – range molecular dynamics, J. Comput. Phys. 117 (1995) 1–19, https://doi.org/10.1006/jcph.1995.1039.
[55] M. Dholakia, S. Chandra, M.C. Valsakumar, S. Mathi Jaya, Atomistic simulations of displacement cascades in Y2O3 single crystal, J. Nucl. Mater. 454 (2014) 96–104, https://doi.org/10.1016/j.jnucmat.2014.07.044.
[56] F. Hanic, M. Hartmanová, G.G. Knab, A.A. Urusovskaya, K.S. Bagdasarov, Real structure of undoped Y2O3 single crystals, Acta Crystallogr. B 40 (1984) 76–82, https://doi.org/10.1107/s0108768184001774.
[57] A.B. Belonoshko, G. Gutierrez, R. Ahuja, B. Johansson, Molecular dynamics simulation of the structure of yttria Y_2O_3 phases using pairwise interactions, Phys. Rev. B Condens. Matter 64 (2001), https://doi.org/10.1103/PhysRevB.64.184103.
[58] M. Dholakia, S. Chandra, S.M. Jaya, Properties of Y2TiO5 and Y2Ti2O7 crystals: development of novel interatomic potentials, J. Alloy. Comp. 739 (2018) 1037–1047, https://doi.org/10.1016/j.jallcom.2017.12.244.
[59] M. Dholakia, S. Chandra, S.M. Jaya, Molecular dynamics studies of displacement cascades in Fe-Y 2 TiO 5 system, in: AIP Conf. Proc., 2016, pp. 1–4, https://doi.org/10.1063/1.4948212.
[60] M.P. Higgins, C.Y. Lu, Z. Lu, L. Shao, L.M. Wang, F. Gao, Crossover from disordered to core-shell structures of nano-oxide Y2O3 dispersed particles in Fe, Appl. Phys. Lett. 109 (2016), https://doi.org/10.1063/1.4959776, 031911.
[61] D.J. Bacon, Y.N. Osetsky, D. Rodney, Dislocation-obstacle interactions at the atomic level, in: Dislocations in Solids, 2009, pp. 1–90, https://doi.org/10.1016/S1572-4859(09)01501-0.
[62] S. Queyreau, J. Marian, M.R. Gilbert, B.D. Wirth, Edge dislocation mobilities in bcc Fe obtained by molecular dynamics, Phys. Rev. B Condens. Matter (2011), https://doi.org/10.1103/PhysRevB.84.064106.
[63] M. Klimiankou, R. Lindau, A. Moslang, HRTEM study of yttrium oxide particles in ODS steels for fusion reactor application, J. Cryst. Growth 249 (2003) 381–387. http://doi.org/10.1016/S0022-0248(02)02134-6.
[64] A. Stukowski, Visualization and analysis of atomistic simulation data with OVITO the open visualization tool, Model. Simul. Mater. Sci. Eng. 18 (2010), https://doi.org/10.1088/0965-0393/18/1/015012, 015012.
[65] T. Lazauskas, S.D. Kenny, R. Smith, G. Nagra, M. Dholakia, M.C. Valsakumar, Simulating radiation damage in a bcc Fe system with embedded yttria nanoparticles, J. Nucl. Mater. 437 (2013) 317–325, https://doi.org/10.1016/j.jnucmat.2013.02.016.
[66] Y. Sun, W. Lai, Molecular dynamics simulations of cascade damage near the Y 2 Ti 2 O 7 nanocluster/ferrite interface in nanostructured ferritic alloys *, Chin. Phys. Lett. B. 26 (2017) 1–7, https://doi.org/10.1088/1674-1056/26/7/076106.
[67] K.D. Hammond, H.-J. Lee Voigt, L.A. Marus, N. Juslin, B.D. Wirth, Simple pairwise interactions for hybrid Monte Carlo–molecular dynamics simulations of titania/yttria-doped iron, J. Phys. Condens. Matter 25 (2013) 55402–55413, https://doi.org/10.1088/0953-8984/25/5/055402.
[68] S. Queyreau, G. Monnet, B. Devincre, Orowan strengthening and forest hardening superposition examined by dislocation dynamics simulations, Acta Mater. 58 (2010) 5586–5595, https://doi.org/10.1016/j.actamat.2010.06.028.
[69] Z. Guo, W. Sha, Quantification of precipitation hardening and evolution of precipitates, Mater. Trans. 43 (2002) 1273–1282, https://doi.org/10.2320/matertrans.43.1273.
[70] S.Y. Hu, S. Schmauder, L.Q. Chen, Atomistic simulations of interactions between Cu precipitates and an edge dislocation in a B . C . C . Fe single crystal, Phys. Status Solidi B 220 (2000) 845–856.
[71] D.J. Bacon, Y.N. Osetsky, Hardening due to copper precipitates in α-iron studied by atomic-scale modelling, J. Nucl. Mater. (2004) 329–333, https://doi.org/10.1016/j.jnucmat.2004.04.256, 1233–1237.
[72] K.C. Russell, L.M. Brown, A dispersion strengthening model based on differing elastic moduli applied to the iron-copper system, Acta Metall. 20 (1972).
[73] D.J. Bacon, U.F. Kocks, R.O. Scattergood, The effect of dislocation self-interaction on the orowan stress, Philos. Mag. A (1973), https://doi.org/10.1080/14786437308227997.
[74] A. Lehtinen, L. Laurson, F. Granberg, K. Nordlund, M.J. Alava, Effects of precipitates and dislocation loops on the yield stress of irradiated iron, Sci. Rep. 8 (2018) 1–12, https://doi.org/10.1038/s41598-018-25285-z.
[75] D. Terentyev, D.J. Bacon, Y.N. Osetsky, Interaction of an edge dislocation with voids in α -iron modelled with different interatomic potentials, J. Phys. Condens. Matter 445007 (2008) 445007, https://doi.org/10.1088/0953-8984/20/44/445007.
[76] M. Peach, J.S. Koehler, The forces exerted on dislocations and the stress fields produced by them, Phys. Rev. 80 (1950), https://doi.org/10.1103/PhysRev.80.436.
[77] W. Cai, V.V. Bulatov, Mobility laws in dislocation dynamics simulations, Mater. Sci. Eng. A 387–389 (2004) 277–281, https://doi.org/10.1016/j.msea.2003.12.085.